

# 顕微鏡用画像統合ソフトウェアにおける AI 技術紹介とライフサイエンス応用

門井宏平, 畑口剛之, 武居俊輔

## Introduction of AI Technology in Imaging Software for Microscopes and Life Science Applications

Kohei KADOI, Takeshi HATAGUCHI and Shunsuke TAKEI

ライフサイエンスの分野で Artificial Intelligence による画像処理の応用が広がりつつある。我々は、顕微鏡システム用の画像統合ソフトウェアである NIS-Elements に、Deep Learning を用いた画像処理技術である NIS.ai を搭載した。NIS.ai は NIS-Elements に統合することで、ユーザーが容易に先進的な Deep Learning 技術を利用することができる特徴を持ち、画像の生成や領域分割の実施が可能である。本稿では NIS.ai の活用により、正確な解析結果の取得とユーザーの作業負荷低減が可能であることを紹介する。まず、非蛍光染色細胞の画像に対し NIS.ai を用いた解析が、蛍光染色細胞の画像を用いた従来の解析と同等の精度となることを確認した。次に、蛍光撮影において問題となる染色試薬による影響や蛍光撮影時に生じる光毒性を NIS.ai の活用により回避出来ることを実証した。最後に、NIS-Elements が制御する顕微鏡撮影手順に NIS.ai を組み込むことにより、従来の画像解析技術の利用では達成が困難であった自動撮影が可能となり、新たな価値を提供できることを示した。

The application of artificial intelligence in image processing is being investigated extensively in life sciences. We developed and installed NIS.ai, an image processing technology that uses deep learning, in NIS-Elements, which is an imaging software for microscope systems. By integrating NIS.ai with NIS-Elements, NIS.ai enables users to use advanced deep learning technology easily with tasks such as image conversion, segmentation and so on. In this study, we show that users can obtain accurate analysis results with minimal effort using NIS.ai. First, we confirm that the analysis using NIS.ai for images of unstained cells exhibits the same accuracy as that of the conventional analysis for images of stained cells. Second, we demonstrate that the effects of staining reagents and the phototoxicity that occurs when capturing fluorescence images can be avoided by utilizing NIS.ai. Finally, we demonstrate that by incorporating NIS.ai into NIS-Elements, automatic imaging, which is difficult to achieve using conventional image analysis, can be achieved, and a new value can be obtained.

**Key words** ライフサイエンス, 顕微鏡, 画像処理, 人工知能, 深層学習  
life science, microscopy, image analysis, artificial intelligence, deep learning

## 1 Introduction

In the field of life science, digital image processing is being conducted during the observation of cells with biological microscopes to automate cell counting and classification. Recently, widespread studies have been conducted on image-processing technology using deep learning, which is a type of artificial intelligence (AI) that is applied to segmentation, classification, digital staining, sharpening, and super-resolution [1].

NIS-Elements is an imaging software for microscope systems with microscope and camera control, image processing, analysis, and reporting functions. Nikon previously equipped NIS-Elements with a microscope image-processing functions,

applying several deep learning techniques. In this paper, we introduce NIS.ai behind the functions that may be adopted for digital staining (Convert.ai) and segmentation (Segment.ai), as well as their applications in life science.

## 2 Microscope image processing functions applying deep learning

Image processing technologies, such as morphological transformation, and non-deep machine learning technologies, such as random forest can be adopted for relatively simple segmentation and sharpening. However, proficient skills and individual adjustments, such as designing image filters, are required to improve the quality of processing results.

The two NIS.ai functions (Convert.ai, Segment.ai) introduced in this paper adopt convolutional neural networks, a type of deep learning, and employ supervised learning, which require training data. Because the design of image filters is automatically performed in its training process, deep learning does not require the traditional image processing or proficient skills required for machine learning. In addition, it is characterized by further improving accuracy by increasing the training dataset size or the number of training iterations.

When using deep learning, hyperparameter usually needs to be tuned, depending on the tasks to be applied. Tuning hyperparameters is a trial-and-error task, which is generally time- and labor intensive. However, since NIS.ai adopts optimized networked construction for microscope images, optimal results can be easily obtained with just a few settings even if the user is not familiar with deep learning.

Table 1 Settings for NIS.ai training

Convert.ai	Iterations
	Dynamic range adaptation (on/off)
Segment.ai	Iterations
	Dynamic range adaptation (on/off)
	Detect touching object (on/off)

Table 1 presents the settings for NIS.ai training. Iterations is an option that specifies the number of training repetitions. Although the optimal value depends on the amount of training data and variations, a value of approximately 1000 is usually acceptable. The training times required to use NVIDIA Quadro RTX 4000 to set 1000 iterations are approximately 3.5 h and 4.0 h with Convert.ai and with Segment.ai, respectively, and the inference time for images of 1600 x 1600 pixels in the same environment is 1 s or less per image. Although the training time is long, this poses no practical challenge because it is more important that a trained model, prepared at one time by the training, can be used several times with a short inference time. “dynamic range adaptation” is an option for specifying when there is little brightness variation in training data, while “detect touching object” is an option for specifying when the user wants a highly-precise isolation of objects in close proximity to each other in Segment.ai.

Processing by NIS.ai comprises two phases: a training phase for preparing a trained model using user-prepared training data, and an inference phase using the training results to output inferred images from the target data (Fig. 1).

In the training phase, the user needs to prepare an original image for conversion, as well as a ground truth image to

serve as a teacher. The image acquisition function of NIS-Elements can acquire multi-channel images such as phase contrast images and fluorescent images. Users can use multi-channel images acquired with NIS-Elements as they are, or use images, which are processed with the NIS-Elements image processing functions, as training data.

In the inference phase, after the target data have been inferred with the trained model, the processing outputs are further processed by the NIS-Elements image processing functions, and analyzed by counting or tracking. Subsequently, the results can be output as graphs or exported to Excel.

In addition, by adopting a function that automates combinations of NIS-Elements standard image processing and analysis processing (GA3), and a function that automates the analysis processing steps from image acquisition with specified complex conditions (JOBS), it is possible to automate the series of processes from image acquisition to analysis. Furthermore, the analysis can be more efficient by changing the processes according to the analysis results. Since NIS.ai is integrated into NIS-Elements, it does not only provide AI-processing for microscope images, but also facilitates highly convenient, automated, and sophisticated analysis.

In the following sections, we introduce examples of NIS.ai applications with such features in life science.

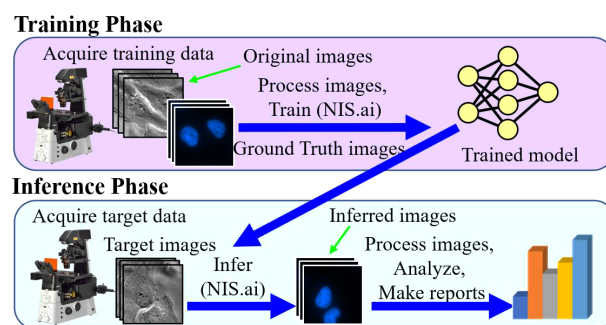


Fig. 1 Processing steps for training and inference

### 3 Examples of AI Applications in the Field of Life Science

This chapter introduces the following three cases using NIS.ai.

- 3.1. Highly accurate fluorescence image generation using unstained microscope images
  - 3.2. Avoiding effects of stain reagents with digital staining
  - 3.3. Automated workflow of acquiring microscope images
- 3.1. Highly accurate fluorescence image generation using unstained microscope images  
 Samples are stained in biology, medical, and drug discov-

ery studies to identify and detect specific structures and molecules in tissue and cells with a microscope. However, staining involves problems such as the cost of reagents, complexity of experiments, and varying staining results. Furthermore, since samples cannot be reused after staining, multiple samples must be prepared during clinical testing. This problem is addressed by adopting deep learning to output stained images of specific structures from unstained microscope images, such as bright field microscopy, which is also called digital staining. The Convert.ai of NIS.ai is a function that can be applied to this digital staining. In this section, we present an example of generating fluorescence images of cell nuclei from images acquired via phase contrast microscopy.

For the verification sample, we adopted a BS-C-1 cell line that constantly expresses the fluorescent-tagged protein localized on the cell nucleus surface. For observation, we used a Ti-E inverted microscope with a 20x objective lens (CFI S Plan Fluor ELWD ADM 20XC 0.45NA, Nikon, Japan), and acquired phase contrast images and fluorescence images with EMCCD (iXon3, Andor technology, Oxford Instruments, UK). Verification proceeded under conditions of 37°C, 5% CO<sub>2</sub>, using a stage-top incubator (STX series, Tokai Hit, Japan) to maintain the culture environment.

Table 2 Summary of training conditions

	Section 3.1	Section 3.2	Section 3.3
Sample used	BS-C-1 cells	HeLa cells	Mouse kidney sections
NIS.ai	Convert.ai		Segment.ai
Training Image	Input	Phase contrast image	Bright field image
	Output	Fluorescence image of cellular nucleus	Glomerular region
Image size	512 x 512 pixels		2048 x 2048 pixels
Number of trained images	70	75	78
Iterations	1000		

For Convert.ai training, we prepared sample images in which the cell density condition was numbered from 20% to 120%, and after training under the conditions presented in Table 2 (Section 3.1 items), we applied the trained model to the time lapse images of a different field of view from the training data. The inference accuracy according to Convert.ai was evaluated based on the growth curve of the number of nuclei and F-score. The growth curve is a graph showing time lapsed alterations in the nuclei number of the same visual field, plotting the quantified number of cell nuclei using existing NIS-Elements image analysis functions.

F-score is a common index that indicates the inference accuracy in machine learning. The closer it is to 1, the higher the accuracy. In addition, it was calculated based on whether or not the center of gravity of cell nuclei in ground truth fluorescence images and Convert.ai inferred the existence of images within 10 pixels.

The obtained results confirmed that localization of cell nuclei inferred by Convert.ai exhibits almost the same localization as ground truth fluorescent images (Fig. 2, white arrowhead). Furthermore, the growth curve also exhibited a curve very close to the results from ground truth, based on fluorescent images, and it verified that the inference accuracy was maintained, even when cell density changed (Fig. 3). It was demonstrated that F-score value for Convert.ai is higher than 0.90, if cell density is up to around 80%. It

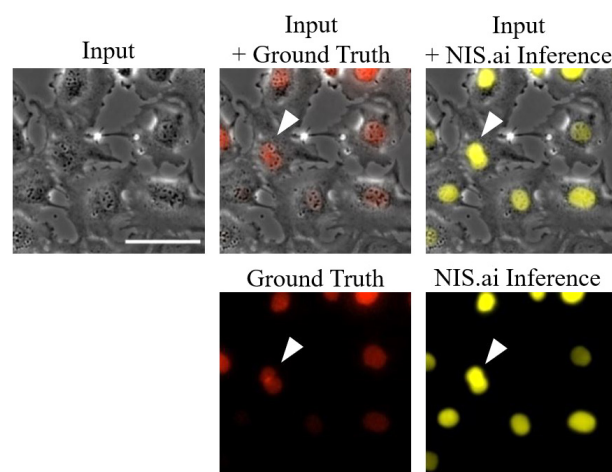


Fig. 2 Comparison of ground truth image of cell nuclei fluorescence and inference image from NIS.ai.

From top left, phase contrast image input into NIS.ai, and input image overlaid with ground truth (red), and input image overlaid with NIS.ai inference (yellow) fluorescence image. Bottom shows ground truth and NIS.ai inferred cell nuclei fluorescence image. White arrowhead indicates the same cell nucleus. Scale bar is 80  $\mu$ m.

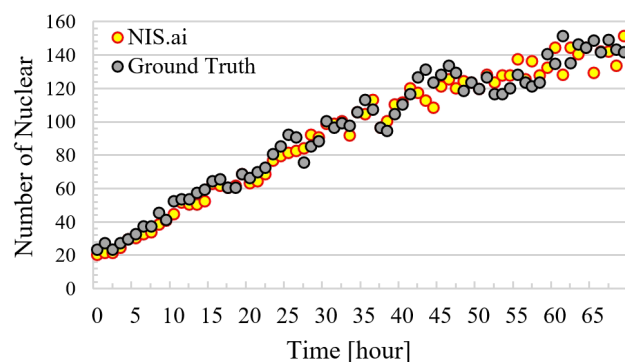


Fig. 3 Comparison of ground truth image of cell nuclei fluorescence, and growth curve of number of cell nuclei using inferred images from NIS.ai.

**Table 3 Accuracy of cell nuclei inference by NIS.ai**

Cell density (%)	Number of cell nuclei					F-score
	Ground truth	NIS.ai	True Positive	False Negative	False Positive	
30	24	22	22	22	0	0.96
50	65	63	62	3	1	0.97
80	73	69	67	6	2	0.94
100	101	99	89	12	10	0.89

was also shown that Convert.ai can infer with high accuracy, if cell density is around 100%, usually difficult to recognize border between cells.

From the above verification results, it can be deduced that by adopting the Convert.ai function of NIS.ai, cell nuclei can be inferred with high accuracy from unstained images with training, using realistic numbers of data. Utilizing NIS.ai can also save the fluorescence wavelength band used in fluorescence microscopy, making it a useful tool for multicolor observation in basic research fields. Furthermore, its use is also anticipated in clinical research in which valuable samples, such as those derived from patient disease tissues, are subject to analysis.

### 3.2. Avoiding effects of stain reagents with digital staining

Sample staining involves problems other than cost, labor, or variations in results between experimenters. Owing to the fact that toxicity caused by the addition of staining reagents and irradiated light for fluorescent images acquisition affects cellular dynamics, it is essential that conditions for reagent use and optical configuration of microscope are sufficiently examined. In addition, in the field of regenerative medicine where cells and tissues are returned to a living body, a problem exists, as the total sample examination with staining cannot be performed. It is possible to circumvent these challenges by adopting fluorescent digital staining with NIS.ai. In this section, we introduce verification results using Hoechst. Hoechst is a widely used staining reagent for cell nuclei detection, and staining with it is known to produce toxic and phototoxic substances [2].

We used HeLa cells for verification samples, and performed image acquisition with the same device configuration and environment for the verification as described in Section 3.1. We prepared two experimental groups to verify the effects of reagents. One was a sample of cell nuclei stained with Hoechst prior to image acquisition (“Stained with Hoechst” group), and the other was an unstained sample

that applied the NIS.ai trained model (“Unstained (NIS.ai)” group). We acquired time lapse images of the two samples, and adopted them for quantitative analysis. Evaluate the inference accuracy of the unstained NIS.ai group, Hoechst staining was performed immediately before the last image acquisition, and ground truth images were acquired. For NIS.ai training data, we separately acquired images of samples with cell density conditions numbered from 20% to 120%, after staining with Hoechst. Subsequently, we prepared a model that trained these images under the conditions in Table 2 (Section 3.2 items) using Convert.ai, and output fluorescent images of cell nuclei from the input phase contrast images. Cell nuclei were detected and quantified for the Hoechst and unstained NIS.ai groups, respectively, and growth curves were prepared.

Based on the obtained results, we found that cells in the stained with Hoechst and unstained NIS.ai groups of comparable density at the start of time lapse were fewer in the stained with Hoechst group than in the unstained NIS.ai group after 60 h, owing to reagents and phototoxicity (Fig. 4). Growth curves also verified that cell growth was suppressed in the stained with Hoechst group (Fig. 5). This indicated that NIS.ai could achieve sufficiently higher accuracy than ground truth images at the final point of the time lapse (Fig. 5, red dot).

These results indicate that correct cell behavior could be observed by fluorescent digital staining using NIS.ai. It is

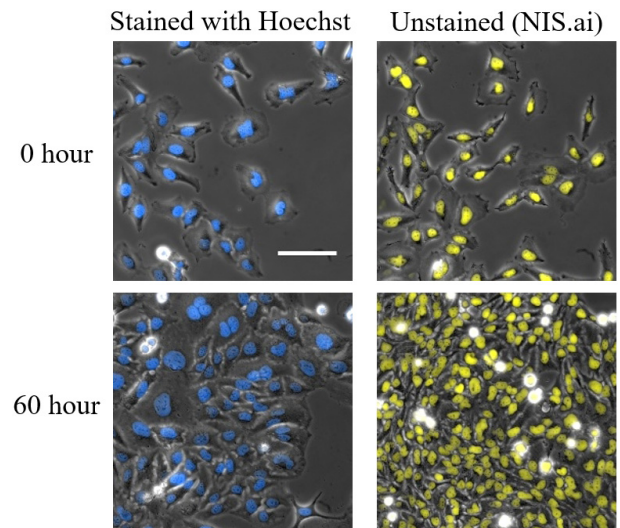


**Fig. 4 Image comparison of cells stained with Hoechst prior to starting image acquisition (left) and unstained cells (right)**

Left and right columns illustrate the cell nuclei regions stained with Hoechst (blue) and inferred by NIS.ai (yellow), respectively, with their respective phase contrast images superimposed over them. Same field of view images at 0 h and 60 h are arranged vertically. Scale bar is 100  $\mu\text{m}$ .

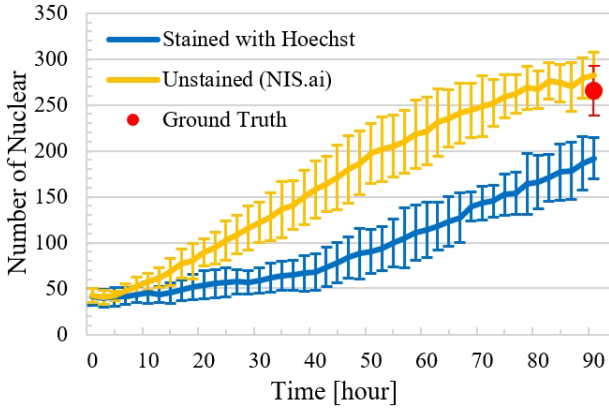


Fig. 5 Comparison of growth curves of number of cell nuclei using cells stained with Hoechst prior to starting image acquisition (blue) and inferred images by NIS.ai of unstained cells (yellow)

Shows the mean  $\pm$  SD ( $n = 3$ ) at each point in time. Unstained cells were stained with Hoechst at the final point, and were considered ground truth (red dot).

assumed that ascertaining the behavior of biological sample precisely, without incurring the effects of staining reagents and phototoxicity, will become increasingly important in the fields of biology, medical science, and drug discovery.

### 3.3. Automated workflow of acquiring microscope images

In studies using conventional microscope images, researchers present only representative microscope images of research subjects, which are often discussed in terms of qualitative results. However, in recent years, technical progress has made it possible to acquire and analyze a large number of images, and it has become necessary to quantitatively evaluate microscope images. Hence, manual image acquisition using a microscope is becoming a serious challenge in case of observing large samples, such as histological sections [3], as well as large-scale screening in drug discovery research [4]. For example, it is known that the specific structure of cells present in the glomerulus is lost in the kidney disease

Table 4 Number of glomerulus detected by NIS.ai and inference accuracy

Ground Truth	NIS.ai	False Negative	False Positive
97	103	1 (1.0%)	7 (7.2%)

nephrotic syndrome [5]. To detect such differences in characteristics, a microscope user needs to use a high-magnification objective lens and acquire images after visually confirming the position of specific structures successively, which places a huge burden on image acquisition and analysis tasks. By incorporating region segmentation by NIS.ai into the image acquisition steps with NIS-Elements, it is possible to narrow down image acquisition regions to specific structures, and thus reduce the burden required of users when conducting image acquisition and analysis. In this section, we present an example of automatically detecting and acquiring the glomerulus images from a kidney section sample.

For verification, we adopted a sample in which a mouse-derived kidney section was treated with Elastica-Masson stain, which tags connective tissues such as elastic and collagen fibers. A Ti2-E inverted microscope equipped with an A1R confocal microscope system was used for image acquisition. For image acquisition, we used a 20x objective lens (CFI Plan Apo Lambda 20X 0.75NA, Nikon, Japan) and CMOS camera (ORCA-Fusion, Hamamatsu Photonics, Japan) to detect the position of the glomerulus. For detailed structural observations, we used a 100x objective (CFI SR HP Apo TIRF 100XC Oil. 1.49NA, Nikon, Japan) and confocal microscope system. We prepared training data, showing a region of the glomerulus in 78 images cut out from full images of two kidney sections obtained by joining multiple images taken with a 20x objective lens. In addition, we constructed a model to output the glomerulus region, according

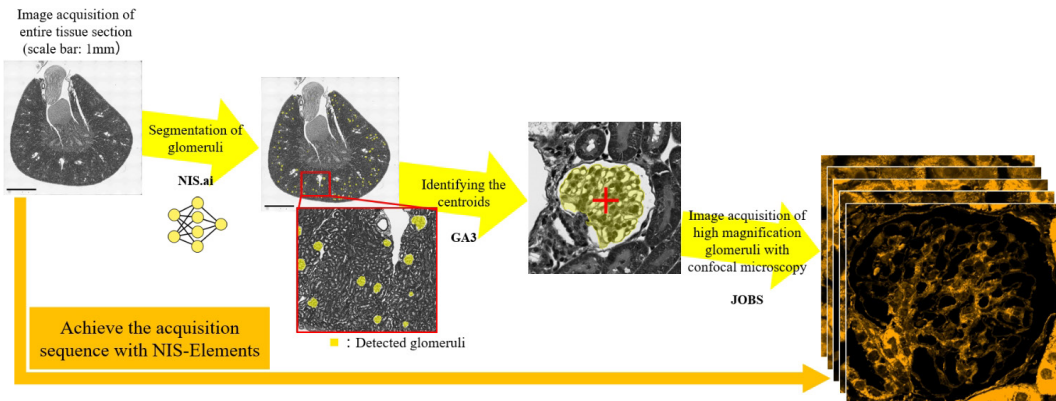


Fig. 6 Overall image of automated workflow from kidney glomerulus detection to high magnification image acquisition.

to the bright field image input from the Segment.ai function (Table 2, Section 3.3 items).

Fig. 6 illustrates a workflow for automating the steps from bright field image acquisition to glomerulus fluorescent image acquisition: 1) construction of kidney total image via bright field image acquisition and stitching, 2) inference of the glomerular region (Segment.ai), 3) calculation of glomerulus center-of-gravity coordinates, and 4) acquisition of glomerulus fluorescent images using a confocal microscope system.

Based on the obtained results, there were a few false positives of the glomerulus region with NIS.ai processing alone; however, only the glomerulus regions were accurately detected by incorporating filter processing, based on area and circularity in GA3 (Fig. 3, red frame). Furthermore, compared to the manual glomerulus detection results, false negatives or positives in NIS.ai processing remained at 1% or 7.2% for each.

From the above, it was demonstrated that regions that are difficult to detect via existing image processing can be accurately detected by NIS.ai. In particular, the lack of false negatives is crucial because in the case of false positives, captured images can be selected later; however, false negative regions need to be re-acquired images. In particular, missing regions that should be detected in clinical testing (for example, detection of cancerous areas) can be fatal. Furthermore, if NIS-Elements is used in combination with NIS.ai to set a sample in a microscope and commence image acquisition, a large number of images can be acquired by the experimenter (user) without being constrained in front of the microscope; hence, drastic labor saving scans can be expected. It is expected that in the future, the acquisition and analysis of large amounts of data for the purpose of quantification will increase in the fields of biology, medicine, and drug discovery. Therefore, the usefulness of automatic image acquisition and image processing workflows utilizing NIS.ai will increase.

## 4 Conclusion

NIS.ai is capable of high-precision digital staining and segmentation, and is effective in applied studies, such as in basic and clinical researches. Although not addressed in this paper, NIS.ai also provides functions for eliminating noise in microscope images and out-of-focus fluorescence leakage. Owing to the combination of these functions and future functional extensions, we further aim to contribute to improving user research efficiency and the discovery of novel findings by providing digital image processing and quantification results that cannot be realized by microscopes alone.

We are grateful to the assistant professor Matsui of the Department of Nephrology, Graduate School of Medicine, Faculty of Medicine, Osaka University, for providing us with mouse kidney-section samples.

## References

- [1] C. Belthangady and L. A. Royer, "Applications, promises, and pitfalls of deep learning for fluorescence image reconstruction," *Nature Methods*, vol. 16, pp. 1215–1225, 2019.
- [2] D. W. Siemann and P. C. Keng, "Cell cycle specific toxicity of the Hoechst 33342 stain in untreated or irradiated murine tumor cells," *Cancer Research*, vol. 46, pp. 3556–3559, 1986.
- [3] O. Zhanmu, X. Yang, H. Gong and X. Li, "Paraffin-embedding for large volume bio-tissue," *Scientific Reports*, vol. 10: 12639, 2020.
- [4] J. R. Lin, M. F. Sichani and P. K. Sorger, "Highly multiplexed imaging of single cells using a high-throughput cyclic immunofluorescence method," *Nature Communications*, vol. 6: 8390, 2015.
- [5] B. Zhu, A. Cao, J. Li, J. Young, J. Wong, S. Ashraf, A. Bierzynska, M. C. Menon, S. Hou, C. Sawyers, K. N. Campbell, M. A. Saleem, J. C. He, F. Hildebrandt, V. D. Dagati, W. Peng and L. Kaufman, "Disruption of MAGI2-RapGEF2-Rap1 signaling contributes to podocyte dysfunction in congenital nephrotic syndrome caused by mutation in MAGI2," *Kidney International*, vol. 96, pp. 642–655, 2019.

門井宏平 Kohei KADOI

ヘルスケア事業部 技術統括部 システム開発部

System Development Department

Technology Solutions Sector

Healthcare Business Unit

武居俊輔 Shunsuke TAKEI

ヘルスケア事業部 技術統括部 システム開発部

System Development Department

Technology Solutions Sector

Healthcare Business Unit

畑口剛之 Takeshi HATAGUCHI

ヘルスケア事業部 技術統括部 設計部

Designing Department

Technology Solutions Sector

Healthcare Business Unit



門井宏平

Kohei KADOI